PHYSICAL REVIEW A **95**, 011404(R) (2017)

Molecular oxygen observed by direct photoproduction from carbon dioxide

Seyedreza Larimian,[1] Sonia Erattupuzha,[1] Sebastian Mai,[2] Philipp Marquetand,[2] Leticia González,[2] Andrius Baltuška,[1] Markus Kitzler,[1] and Xinhua Xie (谢新华)[1,2,*]

[1]*Photonics Institute, Technische Universität Wien, A-1040 Vienna, Austria*

[2]*Institute of Theoretical Chemistry, University of Vienna, A-1090 Vienna, Austria*

(Received 3 May 2016; published 27 January 2017; corrected 10 February 2017)

We report experiments on the direct observation of molecular oxygen formation from CO_2 in strong laser fields with a reaction microscope. Our accompanying simulations and pump-probe measurements suggest that CO_2 molecules undergo bending motion during strong-field ionization which supports the molecular oxygen formation process. The observation of molecular oxygen formation from CO_2 may trigger further experimental and theoretical studies on such processes with laser pulses, and provides hints in studies of the O_2 and O_2^+ abundance in CO_2-dominated planetary atmospheres.

DOI: 10.1103/PhysRevA.95.011404

O_2 production is one of the most important processes for the biosphere of the Earth. Oxygen molecules are mainly generated via photosynthesis by green plants and algae from carbon dioxide and water : $nCO_2 + nH_2O \xrightarrow{\text{light}} (CH_2O)_n + nO_2$ [1]. CO_2 is not only important for the atmosphere on Earth, it is also the dominant compound of the atmosphere on other planets, such as Mars and Venus. One of the most crucial tasks for the quest to establish a human settlement on Mars is the production of O_2 [2]. Because more than 95% of the atmosphere on Mars is CO_2, it will be extremely helpful if O_2 can be produced directly from CO_2. In the past, it was observed that dissociation of CO_2 via absorption of photons leads to a carbon monoxide (CO) and an oxygen atom (O) [3]. However, theoretical simulations suggested the possibility of generating O_2 through the dissociation of a CO_2 molecule [4]. A recent experiment showed indirect evidence of O_2 formation from CO_2 molecules after UV excitation through the detection of C^+ [5]. So far, O_2 formation from CO_2 has not been directly observed.

In the past decade, intense ultrashort laser pulses have been successfully applied to trigger and control molecular reactions such as dissociation and isomerization [6–14]. When a molecule interacts with a strong laser field, electrons from outer molecular orbitals can be excited or removed through tunneling or over-the-barrier ionization, which may prepare the molecule in an excited state or a state with a certain charge. As a consequence, the excited or ionized molecule may undergo severe geometrical reconfigurations and may also break into several fragments or form new chemical bonds. Because of the importance of CO_2 in many research disciplines, strong-field-induced reactions of CO_2 have been experimentally studied with ultrashort lasers by several research groups. However, these studies mainly focused on the topic of ionization and dissociation [15]. In this Rapid Communication, we report on a direct observation of O_2^+ formation straight from CO_2 induced by strong laser pulses with a reaction microscope. Previous studies revealed that neutral O_2 molecules can be conveniently obtained through the neutralization of O_2^+ at metal surfaces [16], which makes the O_2^+ formation method presented here a possible candidate for producing breathable O_2 directly from CO_2. Although the efficiency of the reaction leading to O_2^+ formation is rather low in our measurements, our results can serve as a proof-of-principle experiment on the laser-induced O_2^+ formation directly from CO_2. Our quantum chemical simulations indicate that the bending motion during and after the strong-field interaction plays a critical role in the O_2^+ formation process, which is supported by a Fourier analysis on the O_2 formation yields in our pump-probe measurements.

In the experiments we performed coincidence measurements of ions from doubly ionized CO_2 with a reaction microscope [17]. Laser pulses with a pulse duration (full width at half maximum of the peak intensity) of 25 fs, a central wavelength of 790 nm, a repetition rate of 5 kHz, and peak laser intensities on the order of 10^{14} W/cm^2 are produced with a home-built femtosecond Ti:sapphire laser amplifier system. The reaction microscope consists of a two-stage gas jet arrangement to provide an internally cold ultrasonic gas jet of CO_2 with a diameter of about 170 μm, and an ultrahigh vacuum interaction chamber with a background pressure of 1.0×10^{-10} mbar. The laser beam is focused in the interaction chamber onto the gas jet with a spherical silver mirror with a focal length of 60 mm. A homogeneous dc field of 10.55 V/cm is applied along the axis of the time-of-flight (TOF) spectrometer (z direction) to accelerate positively charged particles to a position-sensitive detector. The laser field is linearly polarized along the spectrometer axis. With the measured position and TOF data, the three-dimensional momentum vector of a certain ion can be retrieved. All possible two-body fragmentation processes can be distinguished using the momentum conservation selection to a pair of ionic fragments. The laser intensities of our measurements are calibrated using the shape of the TOF spectrum of protons from the dissociation of H_2^+ in the strong laser field [18]. More details about the experimental setup can be found in our previous publications [19,20].

We start by focusing on the identification of O_2^+ formation from CO_2^{2+} in our measurements. In Fig. 1(a) we present the TOF spectrum of ions measured when 25 fs laser pulses with a peak intensity of 1.6×10^{14} W/cm^2 interact with isolated CO_2 molecules. The peaks of singly and doubly ionized CO_2 molecules are clearly visible in Fig. 1(a), while two-body fragmentation channels can be unambiguously identified in the photoion-photoion coincidence (PIPICO) distribution. Due to the momentum conservation, two particles

*xinhua.xie@tuwien.ac.at

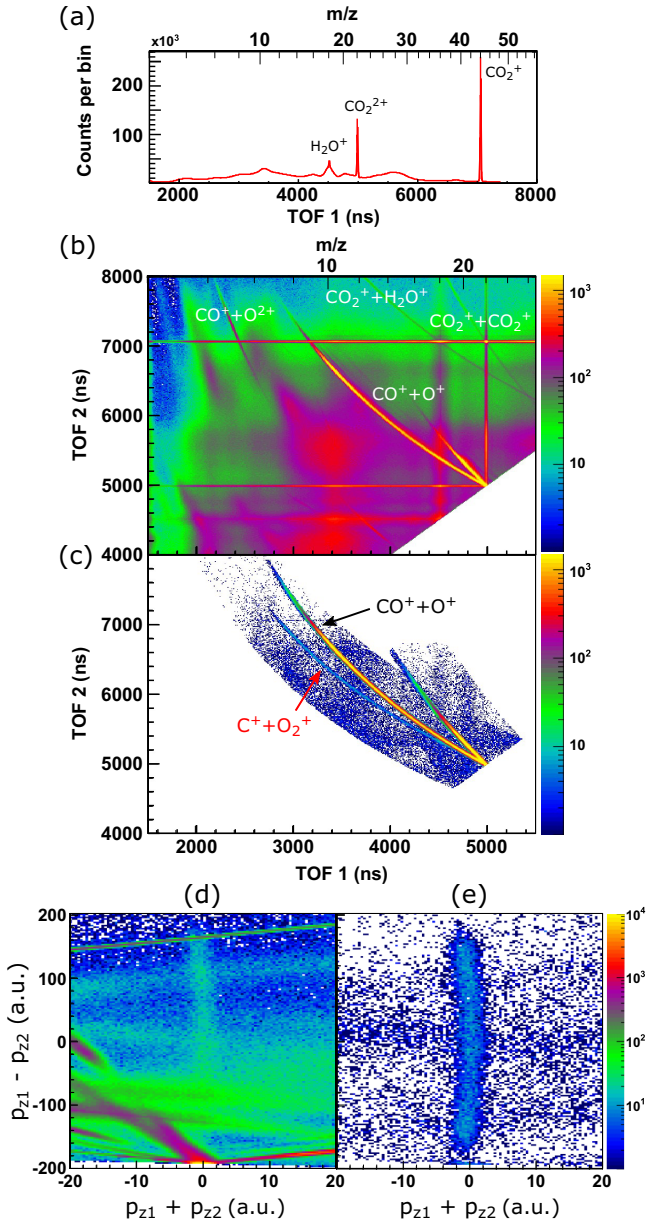

FIG. 1. (a) Measured time-of-flight spectrum of photoions. (b) and (c) present measured photoion-photoion coincidence distributions without and with selection conditions for the two fragmentation channels, respectively. (d) and (e) illustrate momentum correlation distributions for the $C^+ + O_2{}^+$ channel along the laser polarization direction between C^+ and $O_2{}^+$ ions before and after applying the coincidence selection, respectively. The two-body coincidence selection conditions include momentum conservation conditions of $|p_{x1} + p_{x2}| < 2$ a.u. and $|p_{y1} + p_{y2}| < 5$ a.u., and a further condition of $\sqrt{p_{x1}^2 + p_{y1}^2} > 30$ a.u. for the $C^+ + O_2{}^+$ channel to get rid of overlapping with other signals, where the x and y directions are defined along the gas jet and the laser propagation direction, and the indexes 1 and 2 indicate the first and the second considering particles, respectively. These coincidence conditions, together with the momentum conservation condition along the z direction ($|p_{z1} + p_{z2}| < 3$ a.u.), are applied in the data analysis for further studies.

from the same molecule exhibit a correlation between their TOFs, which leads to sharp parabolic lines in the PIPICO distribution [Fig. 1(b)]. The strongest parabolic line in Fig. 1(b)

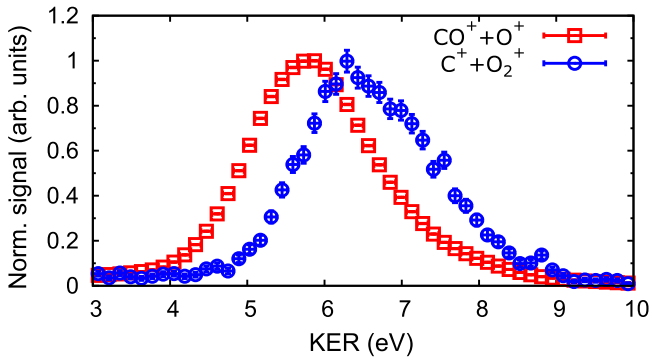

FIG. 2. Kinetic energy release distribution for the $CO^+ + O^+$ channel (red squares) and the $C^+ + O_2{}^+$ channel (blue circles).

is identified as the $CO^+ + O^+$ fragmentation channel. The parabolic line corresponding to a weak fragmentation channel can be enhanced by applying coincidence conditions using the retrieved momentum vectors. The PIPICO distribution with a coincidence selection condition as defined in the caption is depicted in Fig. 1(c), in which the signal corresponding to the formation of the oxygen molecule appears with a high signal-to-noise ratio. Momentum correlation distributions for the $C^+ + O_2{}^+$ channel are shown in Figs. 1(d) and 1(e) before and after applying coincidence conditions. It is clear that in the raw distribution many other signals are superimposed on the signals of the $C^+ + O_2{}^+$ channel. This channel can be well selected by applying coincidence conditions in momentum space, as shown in Fig. 1(e). Our measurements show that the yield of this channel is about three orders of magnitude weaker than that of the $CO^+ + O^+$ channel. Nevertheless, we have directly observed the production of an oxygen molecule from doubly ionized CO_2 in a strong laser field.

From the data selected with the coincidence condition we retrieved the three-dimensional momentum vectors of the two involved ions and calculated the kinetic energy release (KER, the kinetic energy sum of the two ions) of the two observed fragmentation channels. Information about the involved states before the fragmentation can be obtained from the KER distribution of the two-body fragmentation channels, presented in Fig. 2. The KER value is given by the difference between the energies of the initially created dication and the final fragmentation products. The mean values of the KER are 5.9 and 6.6 eV for the $CO^+ + O^+$ channel and the $C^+ + O_2{}^+$ channel, respectively. The width of the KER distribution is related to both the width of the nuclear wave packet and the potential energy surfaces involved in the ionization process. The measured full width at half maxima (FWHM) are about 2.0 eV for both channels, which may suggest that both fragmentation channels originate from an electronic state with a similar curvature.

To gain insight into the $O_2{}^+$ formation mechanism from $CO_2{}^{2+}$, we performed quantum chemical simulations. In order to obtain a balanced and accurate description of all electronic states, we employed a complete active space self-consistent field (CASSCF), augmented by multistate complete active space perturbation theory second order (MS-CASPT2) to include electronic correlation effects [21]. The calculations of potential energy curves were performed within C_{2v} symmetry, with the twofold rotation axis perpendicular to the line

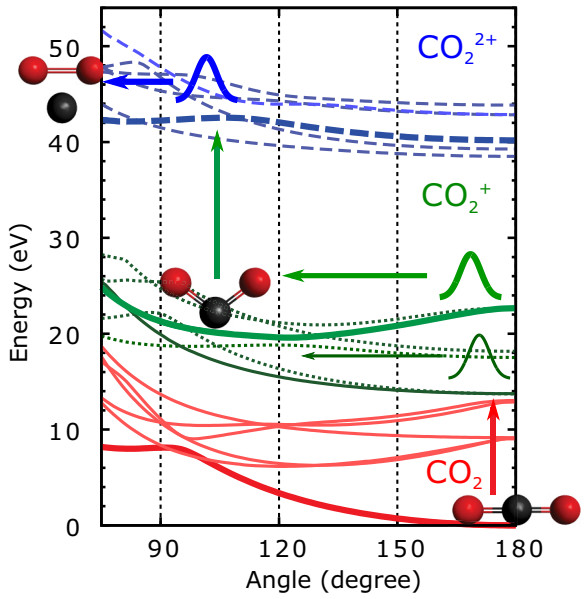

FIG. 3. Simulated potential energy curves for the CO_2 neutral (red lines), the cation (green lines), and the dication (blue lines) over the bending angle. Possible pathways leading to O_2^+ formation are indicated with thick potential energy curves and arrows.

connecting the two oxygen atoms. In this setup, the active space contained four orbitals of a_1 symmetry, three orbitals of b_1, one orbital of a_2, and two orbitals of b_2 symmetry. In the active space, all possible distributions of 12, 11, or ten electrons were considered, respectively, while ten electrons occupied the 2*s* orbitals of oxygen and all 1*s* orbitals. The calculations were performed with MOLCAS 8.0 [22] and the atomic natural orbital type basis with polarization at the triple zeta level (ANO-RCC-VTZP). Note that the calculations did only consider the two lowest states in each symmetry, while Rydberg states were not considered. Figure 3 shows the potential energy curves of these 18 states (six neutral, six cationic, six dicationic) over the bending angle.

To form O_2 from CO_2 the molecule should first form a triangular geometry. There are a number of neutral and cationic states with a gradient pointing towards a bent geometry. Nuclear wave packet dynamics in these excited, intermediate states [23] could thus lead to the bending of the molecule, eventually resulting in the formation of a triangular intermediate. In Fig. 3, we highlight a possible excitation pathway for the dynamics leading to O_2^+ formation through an electronic excited state of CO_2^+: The CO_2 is initially in the neutral ground state (thick red line). Through strong-field nonresonant ionization the system is promoted to an excited state of CO_2^+ (thick green line), which has a minimum at an angle of approximately 120°. Hence, after the first ionization step, the nuclear wave packet evolves towards smaller bending angles, i.e., the molecule starts to bend. When the wave packet crosses the mentioned minimum, the molecule is further ionized to an excited state of CO_2^{2+} (thick blue line), which provides a driving force towards even smaller bond angles. Eventually, in the dicationic state the molecule forms a triangular intermediate, which may release C^+ to form O_2^+. In order to investigate whether bending in CO_2 could be fast enough to occur within the laser pulse duration, we performed simulations using field-free semiclassical dynamics in the first neutral excited state which has a similar shape as the highlighted state of CO_2^+. Indeed, within 25 fs a bending angle of about 110° was reached, which is consistent with our hypothesis that a triangular geometry can form within the pulse duration.

The critical factor leading to the formation of O_2^+ is the bending motion on the cationic state, which can also possibly happen on other electronic states, such as the ground state (*X* state, thin dark green line) of CO_2^+ in Fig. 3. Due to the bandwidth of the femtosecond laser pulse, excited vibrational states can be populated in the strong-field process [24]. The excitation of bending modes in the *X* state can also further lead to the formation of O_2^+, as depicted in Fig. 3.

One should note, however, that due to the influence of the strong laser field, the relevance of the potential energy curves shown in Fig. 3 is somewhat limited. In particular, due to the Stark effect, the potentials may be significantly distorted in a complicated, time-dependent manner. The Stark effect and the difficulties of accurately describing resonant multiphoton absorption and ionization make any prediction of the dynamics of CO_2 during the presence of the laser field extremely difficult. Hence, the potential energy curves only serve for obtaining a qualitative understanding of the O_2^+ formation from the CO_2 dication.

To confirm the mechanism of bending motion-induced O_2 formation, we further performed pump-probe measurements. In the measurements, we used a Mach-Zehnder interferometer with a delay stage in one beam path to control the time delay between the pump and the probe pulses. The scanning step size of the delay stage is set to 0.6 μm, which corresponds to a time delay of 4 fs. The pump and the probe pulses are both linearly polarized along the spectrometer axis with pulse durations of 25 fs and peak intensities of 1.7×10^{14} and 3.0×10^{14} W/cm^2, respectively. The yields of the two fragmentation channels are presented in Fig. 4(a) as a function of the pump-probe delay with normalization to the average yield of each channel separately. The dip at about 100 fs in the yield of the $CO^+ + O^+$ channel is due to the prompt feature in the excitation of a rotational wave packet in CO_2 upon interaction with the first laser pulse [24,25].

To obtain insight into the electronic and nuclear dynamics from the pump-probe measurement, we performed the Fourier transform of the measured yields for the two fragmentation channels in Fig. 4(a). We choose the delay in the range of 333–2667 fs for the Fourier analysis to avoid the influence of the prompt alignment signal. The corresponding frequency resolution is 14 cm^{-1}. The transformed spectra for the $CO^+ + O^+$ channel and the $C^+ + O_2^+$ channel are shown in Figs. 4(b) and 4(c), respectively, which represent frequency components in the measured yield modulations determined by the dynamics induced by the first laser pulse. The Fourier-transformed spectra of the $CO^+ + O^+$ channel has been studied in our previous publication [24]. The strong frequency at 160 cm^{-1} originates from the spin-orbit beating between the doubly degenerate electronic states of CO_2^+, $X\,^2\Pi_{1/2g}$, and $X\,^2\Pi_{3/2g}$ [26]. The other peak at about 1270 cm^{-1} is attributed to the symmetric stretching vibrational dynamics on the *X* state of CO_2^+[26].

The Fourier-transformed spectrum for the O_2 formation channel exhibits several peaks above the noise level. The strongest frequency component is at 508 cm^{-1}, which fits

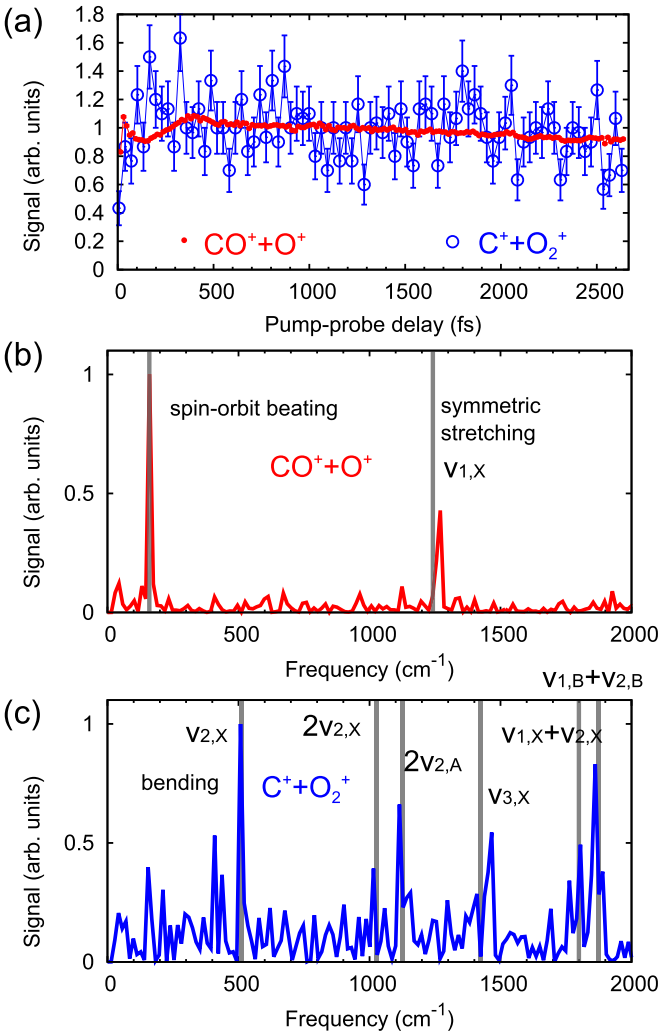

FIG. 4. (a) Normalized signal of the two fragmentation channels as a function of the pump-probe delay. (b) and (c) present Fourier transforms of the measured signal for the $CO^+ + O^+$ channel and the $C^+ + O_2{}^+$ channel, respectively. Vertical lines indicate the transition frequencies from the NIST database [26,27], where ν_1, ν_2, and ν_3 denote the frequencies of the symmetric stretching mode, the bending mode, and the asymmetric stretching mode, respectively. The indexes X, A, and B represent the X, A, and B states of $CO_2{}^+$, respectively.

precisely with the bending frequency (513 cm^{-1}) on the X state of $CO_2{}^+$, while the peaks at 1015 and 1114 cm^{-1} can be assigned to the multiple of the bending frequency on the X state and the A state, respectively [27]. The two peaks at 1805 and 1861 cm^{-1} can be attributed to coupling of the bending modes with the stretching modes on the X state and the A state, respectively [27]. The frequencies from the NIST Chemistry WebBook are indicated as vertical gray lines in Fig. 4(c). The existence of the bending frequencies in Fig. 4(c) indicates that vibrational wave packets with bending motions are populated on the $CO_2{}^+$ state by the pump pulse and such bending motions lead to O_2 formation. These observations are strong evidence that bending motions on the $CO_2{}^+$ state are responsible for the observed O_2 formation process from the laser-induced $CO_2{}^{2+}$. Furthermore, such knowledge manifests that O_2 production efficiency may be enhanced through effectively inducing bending excitation by laser pulses.

In conclusion, we observed the production of $O_2{}^+$ from CO_2 driven by a strong laser pulse with a reaction microscope. Our accompanying quantum chemical simulations suggest that the bending motion during the strong-field interaction may trigger $O_2{}^+$ formation, which is supported by the Fourier analysis on the yield of O_2 formation in pump-probe measurements. Our results may trigger further experimental and theoretical investigations on a deeper understanding of O_2 production from CO_2 and the optimization of the O_2 production efficiency with laser pulses. Moreover, our observation on the $O_2{}^+$ production from $CO_2{}^{2+}$ can also provide useful hints and different concepts for studies on planetary atmospheres. For example, the abundance of O_2 measured on Mars by the Herschel spacecraft [28] and the Curiosity rover [29] may contain the contribution of O_2 formation in the $CO_2{}^{2+}$ layer which is predicted to exist in the atmosphere of Mars [30].

This research was financed by the Austrian Science Fund (FWF) under Grants No. P25615-N27, No. P28475-N27, No. P21463-N22, No. P27491-N27, No. P25827, and No. SFB-F49 NEXTlite, and by a starting grant from the European Research Council (ERC project CyFi). We also acknowledge the Vienna Scientific Cluster (VSC) for providing computational resources and the COST actions CM1204 (XLIC) and CM1405 (MOLIM).

[1] G. S. Singhal, G. Renger, S. K. Sopory, K. D. Irrgang, and Govindjee, *Concepts in Photobiology: Photosynthesis and Photomorphogenesis* (Springer, Berlin, 2012).

[2] M. Hecht, J. Hoffman, MOXIE Team, Lunar and Planetary Science Conference **46**, 2774 (2015).

[3] W. C. Chueh, C. Falter, M. Abbott, D. Scipio, P. Furler, S. M. Haile, and A. Steinfeld, Science **330**, 1797 (2010).

[4] D.-Y. Hwang and A. M. Mebel, Chem. Phys. **256**, 169 (2000); S. Y. Grebenshchikov, J. Chem. Phys. **138**, 224106 (2013).

[5] Z. Lu, Y. C. Chang, Q.-Z. Yin, C. Y. Ng, and W. M. Jackson, Science **346**, 61 (2014).

[6] R. Itakura, K. Yamanouchi, T. Tanabe, T. Okamoto, and F. Kannari, J. Chem. Phys. **119**, 4179 (2003).

[7] M. F. Kling, C. Siedschlag, A. J. Verhoef, J. I. Khan, M. Schultze, T. Uphues, Y. Ni, M. Uiberacker, M. Drescher, F. Krausz, and M. J. J. Vrakking, Science **312**, 246 (2006).

[8] I. Znakovskaya, P. von den Hoff, S. Zherebtsov, A. Wirth, O. Herrwerth, M. J. J. Vrakking, R. de Vivie-Riedle, and M. F. Kling, Phys. Rev. Lett. **103**, 103002 (2009).

[9] D. Geißer, P. Marquetand, J. González-Vázquez, L. González, T. Rozgonyi, and T. Weinacht, J. Phys. Chem. A **116**, 11434 (2012).

[10] A. S. Alnaser, M. Kübel, R. Siemering, B. Bergues, N. G. Kling, K. J. Betsch, Y. Deng, J. Schmidt, Z. A. Alahmed, A. M. Azzeer *et al.*, Nat. Commun. **5**, 3800 (2014).

[11] X. Xie, K. Doblhoff-Dier, S. Roither, M. S. Schöffler, D. Kartashov, H. Xu, T. Rathje, G. G. Paulus, A. Baltuška, S. Gräfe,

and M. Kitzler, Phys. Rev. Lett. **109**, 243001 (2012); X. Xie, K. Doblhoff-Dier, H. Xu, S. Roither, M. S. Schöffler, D. Kartashov, S. Erattupuzha, T. Rathje, G. G. Paulus, K. Yamanouchi *et al.*, *ibid.* **112**, 163003 (2014); X. Xie, S. Roither, M. Schöffler, E. Lötstedt, D. Kartashov, L. Zhang, G. G. Paulus, A. Iwasaki, A. Baltuška, K. Yamanouchi, and M. Kitzler, Phys. Rev. X **4**, 021005 (2014).

[12] P. Marquetand, T. Weinacht, T. Rozgonyi, J. González-Vázquez, D. Geißer, and L. González, in *Advances in Multi-Photon Processes and Spectroscopy* (World Scientific, Singapore, 2014), pp. 1–54.

[13] S. Miura, T. Ando, K. Ootaka, A. Iwasaki, H. Xu, T. Okino, K. Yamanouchi, D. Hoff, T. Rathje, G. G. Paulus *et al.*, Chem. Phys. Lett. **595-596**, 61 (2014).

[14] X. Xie, E. Lötstedt, S. Roither, M. Schöffler, D. Kartashov, K. Midorikawa, A. Baltuška, K. Yamanouchi, and M. Kitzler, Sci. Rep. **5**, 12877 (2015).

[15] W. A. Bryan, J. H. Sanderson, A. El-Zein, W. R. Newell, P. F. Taday, and A. J. Langley, J. Phys. B **33**, 745 (2000); J. P. Brichta, S. J. Walker, R. Helsten, and J. H. Sanderson, *ibid.* **40**, 117 (2007); I. Bocharova, R. Karimi, E. F. Penka, J.-P. Brichta, P. Lassonde, X. Fu, J.-C. Kieffer, A. D. Bandrauk, I. Litvinyuk, J. Sanderson, and F. Légaré, Phys. Rev. Lett. **107**, 063201 (2011); C. Wu, G. Zhang, C. Wu, Y. Yang, X. Liu, Y. Deng, H. Liu, Y. Liu, and Q. Gong, Phys. Rev. A **85**, 063407 (2012).

[16] P. Reijnen, A. Kleyn, U. Imke, and K. Snowdon, Nucl. Instrum. Methods Phys. Res., Sect. B **33**, 451 (1988); N. Lorente and R. Monreal, Surf. Sci. **370**, 324 (1997).

[17] J. Ullrich, R. Moshammer, A. Dorn, R. Dörner, L. P. H. Schmidt, and H. Schmidt-Böcking, Rep. Prog. Phys. **66**, 1463 (2003); R. Dörner, V. Mergel, O. Jagutzki, L. Spielberger, J. Ullrich, R. Moshammer, and H. Schmidt-Böcking, Phys. Rep. **330**, 95 (2000).

[18] A. S. Alnaser, X. M. Tong, T. Osipov, S. Voss, C. M. Maharjan, B. Shan, Z. Chang, and C. L. Cocke, Phys. Rev. A **70**, 023413 (2004).

[19] L. Zhang, S. Roither, X. Xie, D. Kartashov, M. Schöffler, H. Xu, A. Iwasaki, S. Gräfe, T. Okino, K. Yamanouchi *et al.*, J. Phys. B **45**, 085603 (2012).

[20] X. Xie, S. Roither, D. Kartashov, E. Persson, D. G. Arbó, L. Zhang, S. Gräfe, M. S. Schöffler, J. Burgdörfer, A. Baltuška, and M. Kitzler, Phys. Rev. Lett. **108**, 193004 (2012).

[21] P. Pulay, Int. J. Quantum Chem. **111**, 3273 (2011); K. Andersson and B. O. Roos, in *Modern Electronic Structure Theory, Part I*, edited by D. R. Yarkony (World Scientific, Singapore, 1995), pp. 55–109; B. O. Roos, in *Theory and Applications of Computational Chemistry*, edited by C. E. Dykstra, G. Frenking, K. S. Kim, and G. E. Scuseria (Elsevier, Amsterdam, 2005), pp. 725–764; J. Finley, P.-Å. Malmqvist, B. O. Roos, and L. Serrano-Andrés, Chem. Phys. Lett. **288**, 299 (1998).

[22] F. Aquilante, J. Autschbach, R. K. Carlson, L. F. Chibotaru, M. G. Delcey, L. De Vico, I. Fdez. Galván, N. Ferré, L. M. Frutos, L. Gagliardi *et al.*, J. Comput. Chem. **37**, 506 (2016).

[23] P. Sándor, V. Tagliamonti, A. Zhao, T. Rozgonyi, M. Ruckenbauer, P. Marquetand, and T. Weinacht, Phys. Rev. Lett. **116**, 063002 (2016).

[24] S. Erattupuzha, S. Larimian, A. Baltuška, X. Xie, and M. Kitzler, J. Chem. Phys. **144**, 024306 (2016).

[25] J. Ortigoso, M. Rodriguez, M. Gupta, and B. Friedrich, J. Chem. Phys. **110**, 3870 (1999); F. Rosca-Pruna and M. J. J. Vrakking, Phys. Rev. Lett. **87**, 153902 (2001).

[26] P. Baltzer, F. T. Chau, J. H. D. Eland, L. Karlsson, M. Lundqvist, J. Rostas, K. Y. Tam, H. Veenhuizen, and B. Wannberg, J. Chem. Phys. **104**, 8922 (1996); J. Liu, W. Chen, C.-W. Hsu, M. Hochlaf, M. Evans, S. Stimson, and C. Y. Ng, *ibid.* **112**, 10767 (2000).

[27] P. Linstrom and W. Mallard, NIST Chemistry WebBook, NIST Standard Reference Database Number 69, http://webbook.nist.gov/chemistry/.

[28] P. Hartogh, C. Jarchow, E. Lellouch, M. de Val-Borro, M. Rengel, R. Moreno, A. Medvedev, H. Sagawa, B. Swinyard, T. Cavalié *et al.*, Astron. Astrophys. **521**, L49 (2010).

[29] P. R. Mahaffy, C. R. Webster, S. K. Atreya, H. Franz, M. Wong, P. G. Conrad, D. Harpold, J. J. Jones, L. A. Leshin, H. Manning *et al.*, Science **341**, 263 (2013).

[30] O. Witasse, O. Dutuit, J. Lilensten, R. Thissen, J. Zabka, C. Alcaraz, P.-L. Blelly, S. W. Bougher, S. Engel, L. H. Andersen, and K. Seiersen, Geophys. Res. Lett. **29**, 104-1 (2002).